Chemistry Europe
European Chemical Societies Publishing

WILEY VCH

Excellence in Chemistry Research

Announcing our new flagship journal

- Gold Open Access
- Publishing charges waived
- Preprints welcome
- Edited by active scientists

Meet the Editors of *ChemistryEurope*

Luisa De Cola
Università degli Studi di Milano Statale, Italy

Ive Hermans
University of Wisconsin-Madison, USA

Ken Tanaka
Tokyo Institute of Technology, Japan

Chemistry–A European Journal
Research Article
doi.org/10.1002/chem.202300637
Chemistry Europe
European Chemical Societies Publishing
www.chemeurj.org

Bonding in Low-Coordinated Organoarsenic and Organoantimony Compounds: A Threshold Photoelectron Spectroscopic Investigation

Emil Karaev,[a] Marius Gerlach,[a] Lukas Faschingbauer,[a] Jacqueline Ramler,[b] Ivo Krummenacher,[c] Crispin Lichtenberg,*[b] Patrick Hemberger,*[d] and Ingo Fischer*[a]

Dedicated to Prof. Dr. Hansjörg Grützmacher in honour of his contributions to p-block chemistry.

Abstract: Methyl and methylene compounds of arsenic and antimony have been studied by photoelectron photoion coincidence spectroscopy to investigate their relative stability. While for As both HAs=CH_2, As–CH_3 and the methylene compound As=CH_2 are identified in the spectrum, the only Sb compound observed is Sb–CH_3. Thus, there is a step in the main group 15 between As and Sb, regarding the relative stability of the methyl compounds. Ionisation energies, vibrational frequencies and spin-orbit splittings were determined for the methyl compound from photoion mass-selected photoelectron spectra. Although the spectroscopic results for organoantimony resemble those for the previously investigated bismuth compounds, EPR spectroscopic experiments indicate a far lower tendency for methyl transfer for $Sb(CH_3)_3$ compared to $Bi(CH_3)_3$. This study concludes investigations on low-valent organopnictogen compounds.

Introduction

Elements E of the main group 15 (pnictogens, E–N–Bi) favour high oxidation states like −3 (especially for E–N), +3 and +5.[1] In particular, the heavier congeners As, Sb and Bi are present in the oxidation state +3 in most of their molecular compounds. Non-stabilised low-valent compounds with E in a low oxidation state such as +1 are generally highly reactive, electron deficient and difficult to isolate.[2] However, they can appear as chemical intermediates in numerous reactions (see examples below) and can be expected to differ from their Lewis base-stabilised analogues,[3] therefore a characterisation of their electronic structure is of considerable interest. In recent years, we started a systematic investigation of reactive species E–CH_3 in the gas phase, using threshold photoelectron spectroscopy (TPES).[4] When E–N, a N=C double bond is formed and methanimine HN=CH_2 is by far the most stable isomer, while N–CH_3 has not yet been observed.[5] In contrast, methylbismuth has been characterised as a bismuthinidene biradical Bi–CH_3 with a triplet ground state.[2f] For E–P, the methylene species HP=CH_2 is also the most stable isomer, but P–CH_3 is only 0.65 eV higher in energy and both have recently been identified in a photoelectron spectrum.[2e] This raises the question at which position in group 15 the methyl compound (E–CH_3) becomes more stable than the methylene species (HE=CH_2) and dominates the spectra. To address this question, we synthesised methyl and methylene compounds of arsenic and antimony in situ from their respective $E(CH_3)_3$ precursors using a pyrolysis reactor and obtained mass spectra of the decomposition products and high-resolution threshold photoelectron spectra.

Although of fundamental importance for describing bonding in low-valent group 15 compounds, this is not a purely academic question. For example, low-valent organoantimony species have been suggested to be generated as intermediates in the transition metal-catalysed liberation of dihydrogen from stibanes[6] and low-valent bismuth compounds have been shown to engage in Bi^{I}/Bi^{III} redox cycles for reactions such as the hydrodefluorination of arenes.[7] Furthermore, organoantimony compounds are used in semiconductor materials and solar cells.[8] Here, the isomer-selective identification of inter-

[a] E. Karaev, M. Gerlach, L. Faschingbauer, Prof. Dr. I. Fischer
Institute of Physical and Theoretical Chemistry
Julius-Maximilians-Universität Würzburg
Am Hubland, 97074 Würzburg (Germany)
E-mail: ingo.fischer@uni-wuerzburg.de
[b] Dr. J. Ramler, Prof. Dr. C. Lichtenberg
Department of Chemistry
Philipps-University of Marburg
Hans-Meerwein-Str. 4, 35032 Marburg (Germany)
E-mail: crispin.lichtenberg@chemie.uni-marburg.de
[c] Dr. I. Krummenacher
Institute of Inorganic Chemistry, University of Würzburg
Am Hubland, 97074 Würzburg (Germany)
[d] Dr. P. Hemberger
Laboratory for Synchrotron Radiation and Femtochemistry
Paul Scherrer Institut (PSI)
5232 Villigen (Switzerland)
E-mail: patrick.hemberger@psi.ch

Supporting information for this article is available on the WWW under https://doi.org/10.1002/chem.202300637

Part of a Special Collection on the p-block elements.

mediates that are formed in the thermolysis of organo-antimony precursors is crucial for understanding the mechanism of chemical vapour deposition (CVD).[8b,9] So far, the amount of information on reactive Sb and As species is limited. For methylenearsane, an ionisation energy (IE) of 9.7 eV has been determined in a dispersive He (I) photoelectron spectrum,[10] in reasonable agreement with computations.[11] Not all bands in the spectrum were assigned and vibrational resolution was not achieved. In computations for E–CH_3 (E–N, P, As) that included spin-orbit coupling, a triplet ground state was found.[12] Bond lengths to carbon were predicted for E–As and Sb by simple Hartree-Fock calculations.[13]

Due to its sensitivity to the character of electronic states and the isomeric structure, photoelectron spectroscopy is well suited to describe the electronic structure of molecules. Here, we employ threshold photoelectron-photoion coincidence spectroscopy (PEPICO).[14] Ion mass-selected threshold photoelectron spectra, ms-TPES, for different species can be extracted from the full data set. The technique is thus well-suited for studying photoelectron spectra of reactive species in complex mixtures.[15]

Results

Arsenic

To identify the pyrolysis products of $As(CH_3)_3$, time of flight (TOF) mass spectra have been recorded at different pyrolysis temperatures and photon energies. In Figure 1, mass spectra of $As(CH_3)_3$ recorded at 10 eV are depicted. Without pyrolysis (upper trace) only the precursor *m/z* 120 is detected, as well as some contaminants from previous experiments (acetone and iodine), thus there is no dissociative photoionisation of the precursor observed, in agreement with the previously reported onset of methyl loss from $As(CH_3)_3$ of 10.620 eV.[16] By increasing

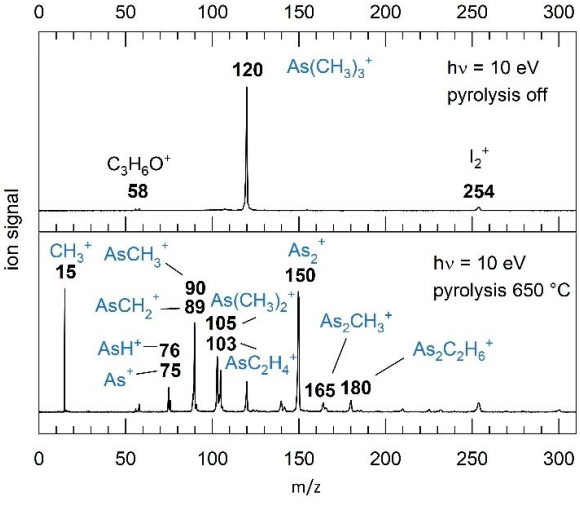

Figure 1. TOF mass spectra at 10 eV photon energy of the precursor $As(CH_3)_3$ (top) and its pyrolysis products at 650 °C (bottom). Acetone (*m/z* 58) and I_2 (*m/z* 254) are present as contaminants from previous experiments.

the pyrolysis to 650 °C (lower trace), several fragments from thermal decomposition are observed.

A strong signal of *m/z* 15 shows the formation of methyl radicals, while the masses at *m/z* 105 ($As(CH_3)_2$), 90 (As–CH_3) and 75 (As) indicate a stepwise methyl abstraction [Eq. (1)]:

$$As(CH_3)_3 \xrightarrow{-CH_3} As(CH_3)_2 \xrightarrow{-CH_3} As(CH_3) \xrightarrow{-CH_3} As \qquad (1)$$

However, a mass spectrum recorded at 12 eV also shows peaks corresponding to C_2H_6 and C_2H_4, which indicates the presence of additional concerted reaction pathways associated with loss of ethane or ethene. A signal of *m/z* 89 suggests decomposition of the species associated with *m/z* 105 into methane and As–CH_2 or H loss from the species associated with *m/z* 90. A further H-atom loss is indicated by the appearance of As–CH (*m/z* 88). An expanded view of the mass region between *m/z* 85 and 95 is given as Figure S1 in the Supporting Information and shows that the mass peaks can be well separated. M/z 103 most likely arises from a consecutive H_2 loss of *m/z* 105 and was already assigned to AsC_2H_4 with a bridged ethene structure.[16] The signal at *m/z* 76 is likely due to reaction of As with a hydrogen atom and not by methylene loss from the compound detected at *m/z* 90, since no signal of *m/z* 14 is observed at higher photon energies. Furthermore, the higher masses *m/z* 150, 165 and 180 are dimerisation products of two As atoms (*m/z* 150), As and As–CH_3 (*m/z* 165), and two As–CH_3 fragments (*m/z* 180), respectively. In addition, *m/z* 300 is observed and corresponds to an As tetramer.

To gain structural information of the pyrolysis products, ion-mass selected threshold photoelectron (ms-TPE) spectra were recorded. Here, we will focus on the ms-TPE spectra of *m/z* 90 and 89. Dispersive photoelectron spectra have already been reported for group 15 dimers[17] and tetramers,[18] and no additional information is available from our work. Therefore, their spectra as well as the unstructured ones of the species As_2R_x are only given as Figure S2. On the other hand, TPE-spectra of AsH and AsCH will be discussed in a future publication.

Figure 2 shows the ms-TPE spectrum of *m/z* 90. Three major bands are observed, the first two being associated with a vibrational progression. A simulated spectrum of As–CH_3 based on DFT (B3LYP\6-311G(2d,d,p)) computations (green) was found to fit only the low energy part of the first band from 8.5 to 9.2 eV. The computed ionisation energy (IE) of 8.80 eV matches the observed IE of 8.70 eV well. A small band at 8.64 eV is assigned to a hot band transition. As has been pointed out before, As–CH_3 has a X $^3A_2$ ground state with a C_{3v} symmetry.[12] The two unpaired electrons are located in two p-orbitals (SOMO, singly occupied molecular orbitals) at the As. Although formally non-bonding, removal of an electron from the SOMO leads to shortening of $R_{(AsC)}$ from 1.98 to 1.89 Å (Table 1). Computations yielded a slightly tilted CH_3 group relative to the As–C bond in the ion and an elongation of one of the C–H bonds, which causes a symmetry reduction to C_s. However, the calculated pseudo rotational barrier of the CH_3 group is 72 meV, while the zero point energy amounts to 918 meV. Therefore, the CH_3 group in As–CH_3^+ can freely rotate and an effective C_{3v}

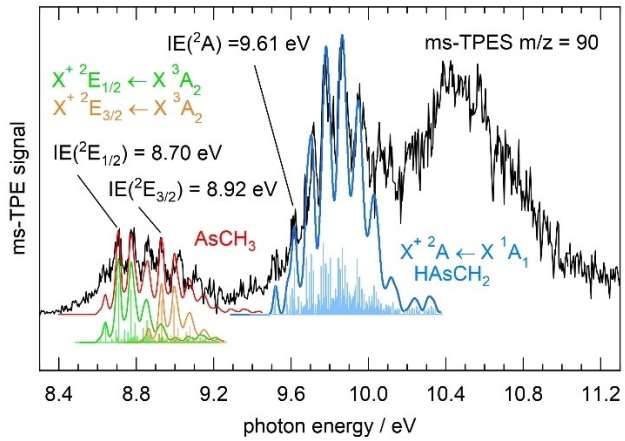

Figure 2. Ms-TPES of *m/z* 90 (black) with FC simulations for comparison. The red line represents the sum of the simulations for the $X^+\,^2E_{1/2}\leftarrow X\,^3A_2$ (green) and $X^+\,^2E_{3/2}\leftarrow X\,^3A_2$ (orange) transitions in As–CH_3. The blue line is a fit to the $X^+\,^2A\leftarrow X\,^1A_1$ transition of HAs=CH_2. The third band maximising at 10.5 eV is most likely due to a transition into the excited A $^2A'$ state of HAs–CH_2^+.

Table 1. Computed minimum-energy geometries of As–CH_3 in its X $^3A_2$ and As–CH_3^+ in its $X^+\,^2E_{1/2}/^2E_{3/2}$ states.

	X $^3A_2$	$X^+\,^2E_{1/2}/^2E_{3/2}$
$R_{(AsC)}$/Å	1.98	1.89
$R_{(CH)}$/Å	3×1.09	2×1.09 1.11
$\theta_{(As-CH)}$/°	3×110	2×113 103
$\theta_{(HCH)}$/°	3×109	2×107 113

symmetry results. Spin-orbit calculations using NEVPT2 [11,11] revealed an energy difference of 220 meV for the splitting of the cationic ^2E state into the $^2E_{1/2}$ and $^2E_{3/2}$ components. NEVPT2 (N-electron valence state second order perturbation theory) is an alternative to the well-known CASPT2 method and tends to yield more accurate excitation energies.[19] Relativistic effects were included by choosing a relativistic basis set and using the Douglas-Kroll-Hesse (DKH) method,[20] The value of 220 meV matches almost exactly the energy difference between the IE of 8.70 and the band at 8.92 eV that is severely underestimated in intensity in the simulation (green). This indicates that the $X^+\,^2E_{3/2}\leftarrow X\,^3A_2$ progression overlaps with the $X^+\,^2E_{1/2}\leftarrow X\,^3A_2$ (orange) transition. The best simulation of both transitions (red) was obtained when the vibrational band at 8.92 eV was assigned to the origin transition into the upper spin-orbit component and the intensity of transitions into the lower spin-orbit component was weighted by a factor of 1.4. The vibrational progression is dominated by two modes, the CH_3-wagging mode $\tilde{\nu}_9^+$, computed at 520 cm^{-1} and the (approximate) As–C stretching mode $\tilde{\nu}_7^+$ =670 cm^{-1}. Note that the geometry of the individual spin-orbit components was not further optimised.

The somewhat inferior fit at higher energies indicates that the vibrational modes of the $^2E_{3/2}$ state have a slightly lower frequency compared to $^2E_{1/2}$. Table 1 summarises the computed minimum energy geometries of the neutral and the ionic ground state, without considering spin-orbit splitting.

The second band from 9.5 to 10.2 eV is assigned to the constitutional isomer HAs=CH_2^+. This transition has been reported before[10] and an IE of 9.7 eV was derived. However, in the previous work vibrational resolution[10] was not achieved, while the present spectrum shows a long and intense progression with a spacing of roughly 700 cm^{-1}. Simple DFT computations indicate that neutral HAs=CH_2 is the more stable isomer and 136 meV lower in energy than As–CH_3. The FC simulation on the CBS-QB3 level of theory (blue line) fits the experimental data very well. It is based on the computed geometry given in Table 2. The deviations at energies above 10 eV are most likely due to the onset of the third band. The transition at 9.61 eV is assigned to the IE of HAs=CH_2, in good agreement with the value of 9.79 eV obtained in CBS-QB3 computations. According to the computations, the neutral ground state is a planar singlet with a double minimum potential along the C–As–H angle $\theta_{(HAsC)}$, thus HAs=CH_2 is C_s symmetric, similar to methanimine. Upon ionisation, the dihedral angle $\phi_{(HAs-CH)}$ changes from 0° in the neutral compound to 34° in the cation, thus the cation becomes non-planar. The most important geometry parameters of HAs=CH_2 and its cation are listed in Table 2. The ionisation can be described as a $D_0^+\leftarrow X\,^1A'$ transition, with an electron being ejected from the π_{As-C} (A'') orbital,[10] associated with an increase in $\Delta R_{(AsC)}$ of +0.03 Å. The observed vibrational progression of ≈700 cm^{-1} cannot be assigned to a single mode, but is composed of four different low-frequency vibrational modes with computed values of $\tilde{\nu}_6^+$ =790 cm^{-1}, $\tilde{\nu}_7^+$ =710 cm^{-1} (out of plane bend), $\tilde{\nu}_8^+$ =620 cm^{-1} (in plane bend), $\tilde{\nu}_9^+$ =500 cm^{-1} (CH_2 torsion). All four vibrations show some As–C stretching character and are depicted in Table S1. Above 10.2 eV, a further unstructured band is apparent that extends to around 11 eV and has also been observed previously.[10] It is assigned to the transition into the excited A $^2A'$ state of HAs–CH_2^+ due to ionisation of a non-bonding electron in the n_{As} (A') in accordance with the prior work and our own calculations that yield a vertical excitation energy in the ion of +0.62 eV. As a different precursor was used by Chrostowska et al., a significant contribution from dissociative ionisation to the band is unlikely (Figure S3). However, a small contribution from the first excited state of $AsCH_3^+$ to the band is possible. Based on our computations it is expected to appear at 10.78 eV.

Figure 3 depicts the ms-TPES of *m/z* 89, corresponding to As=CH_2 at an elevated pyrolysis temperature of around 800 °C.

Table 2. Computed minimum energy geometries of HAs–CH_2 in its X $^1A'$ and HAs–CH_2^+ in its D_0^+ state.

	HAs–CH_2	HAs–CH_2^+
$R_{(AsC)}$/Å	1.86	1.89
$\phi_{(HAs-CH)}$/°	0	34
$\theta_{(As-CH)}$/°	124 119	2×121
$\theta_{(H-C)}$/°	96	94

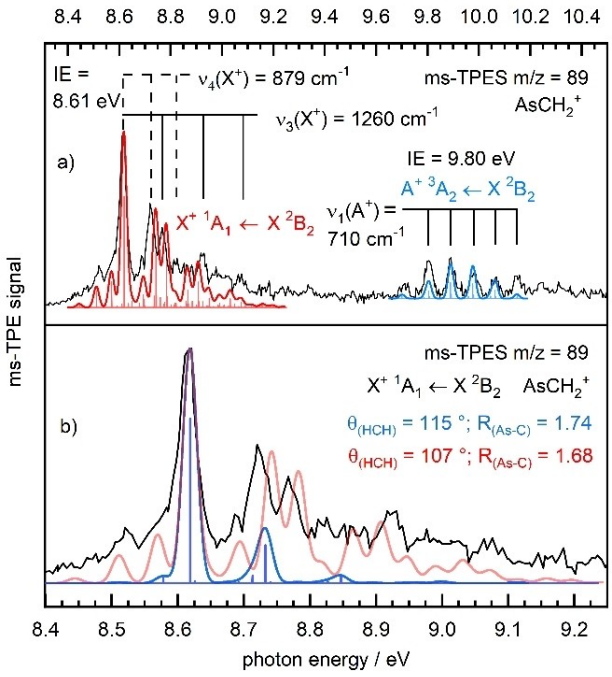

Figure 3. Ms-TPES of *m/z* 89, As–CH_2^+ (black line). a) complete spectrum with simulations for the $X^+\,^1A_1 \leftarrow X\,^2B_2$ (red) and $A^+\,^3A_2 \leftarrow X\,^2B_2$ (blue) transition. The former simulation was adjusted as described in the text. b) Close-up of the $X^+\,^1A_1 \leftarrow X\,^2B_2$ transition with the calculated (blue) and adjusted (red) geometries.

It features two separate transitions between 8.4 and 9.2 eV and from 9.7 to 10.3 eV.

While trace (a) depicts the complete spectrum, trace (b) is a close-up of the lower energy transition. Again, FC-simulations based on quantum chemical calculations helped to rationalise the spectrum. Neutral As=CH_2 is C_{2v} symmetric with a $X\,^2B_2$ electronic ground state. The intense band at 8.61 eV fits well with the calculated IE for the $X^+\,^1A_1 \leftarrow X\,^2B_2$ transition of As=CH_2 of 8.56 eV at the CCSD(T) level of theory. However, the FC-simulations based on a variety of computational approaches, including the MP2, MP4, CCSD(T), DFT and CASSCF methods deviated from the experiment and the intensity of the bands at higher energy, in particular the band at 1260 cm^{-1} was significantly underestimated by all methods (Figure 3b (blue) and Table S2). The wavenumber of the symmetric CH_2 bending was indeed computed around 1300 cm^{-1}, depending on the method. However, the FC simulations yielded only negligible intensity for this mode. We again included relativistic effects in our calculations by choosing a relativistic basis set and using the DKH method,[20] which also had negligible influence on the structure and FC-simulation. Different constitutional isomers, including H_2As=C and HAs–CH were calculated using the G4 approach, but neither the computed IEs of 9.47 and 12.9 eV nor their vibrational structure matched the experimental spectrum. Note that the cationic ground state is of singlet multiplicity, so spin-orbit splitting is not relevant.

On the other hand, the FC simulation for the transition into the first excited state $A^+\,^3A_2$ based on CBS-QB3 computations (blue line) agrees very well with the experiment. An ionisation energy of 9.80 eV is derived from the simulation, in good agreement with the calculated value of 9.89 eV. The band is dominated by the As–C stretching vibration $\tilde{\nu}_6^+ = 710\ cm^{-1}$ and a feature around 9.70 eV is assigned to a hot band. The electron is removed from a σ orbital with As–C bonding character, which results in an increase of $R_{(AsC)}$ from 1.77 Å in the neutral species to 1.89 Å in the cation and thus explains the activity in the As–C stretch. Since the transition into the triplet state is well simulated, the geometry and force constants of neutral As=CH_2 should be correct. Furthermore, transitions from excited states in the neutral compound should not contribute. The reason for the deviations in the transition to the $X^+\,^1A_1$ state lies therefore in the representation of the ionic state. Also, note that the first excited singlet cationic state lies 1.8 eV above the cationic ground state according to TDDFT calculations.

The first explanation for the initial difficulties to interpret the overall spectrum shown in Figure 3 is perturbation of band intensities by autoionisation. The deviations might then be explained by the enhancement of vibrational transitions, in particular the symmetric CH_2-bending mode, due to interactions with resonantly excited autoionising states.[21] No peaks were identified in the photoion yield at the corresponding photon energies. Constant ionic state spectra might confirm the presence of autoionisation in the spectrum.[22]

However, there is also a second possible explanation: a potential energy surface scan revealed a flat potential along the bending coordinate around the minimum energy geometry. We therefore modified the geometry of As–CH_2^+ in its $X^+\,^1A_1$ state in order to empirically improve the FC fit of the experimental spectrum and manually varied the angle $\theta_{(HCH)}$ as well as $R_{(AsC)}$ until the best fit with the spectrum was obtained. The FC-simulation shown as a red line in Figure 3a and b was obtained with $\theta_{(HCH)} = 107°$ and $R_{(AsC)} = 1.68$ Å, and fits the experimental spectrum much better. The experimentally observed wavenumbers for the modes $\tilde{\nu}_4^+ = 1260\ cm^{-1}$ (HCH in plane bend) and $\tilde{\nu}_3^+ = 880\ cm^{-1}$ (AsC stretch) are slightly lower than the calculated ones of $\tilde{\nu}_{4\,calc}^+ = 1300\ cm^{-1}$ and $\tilde{\nu}_{3\,calc}^+ = 1000\ cm^{-1}$, respectively (DFT, ωB97-XD/aug-cc-pVTZ). However, the geometry parameters are substantially different from the computed values for the minimum of $\theta_{(HCH)} = 115–117°$ and $R_{(AsC)} = 1.72–1.75$ Å. As the energy difference between the best fit geometry and the global minimum was computed to be only 61 meV, the harmonic approximation might be inappropriate for a good fit of the experimental spectrum.

Antimony

For the investigation of antimony compounds, very similar strategies were employed. Trimethylantimony, $Sb(CH_3)_3$ has been pyrolysed under very similar conditions as the arsenic compound. Figure 4 shows two mass spectra recorded at 9 eV photon energy. Dissociative photoionisation is not evident in the ion images at 9 eV (see the Supporting Information S3) because the appearance energy $AE_{0K}(Sb(CH_3)_3, Sb(CH_3)_2^+)$ is 9.9 eV.[16]

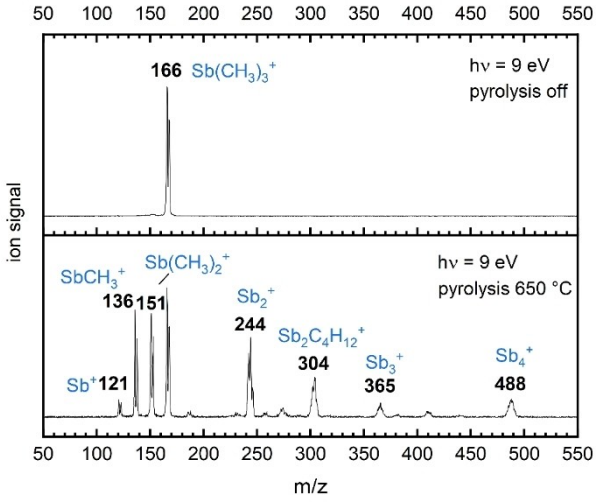

Figure 4. TOF mass spectra of the precursor $Sb(CH_3)_3$ (top) and its pyrolysis products at 650 °C (bottom) at 9 eV photon energy.

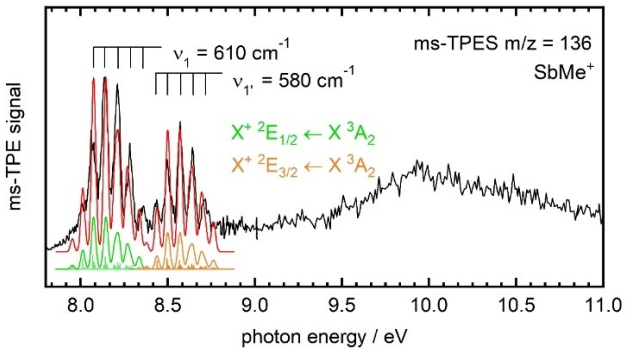

Figure 5. Ms-TPES of *m/z* 136, $Sb–CH_3^+$ (black). The red line represents a FC simulation of the $X^+\,^2E_{1/2}\leftarrow X\,^3A_2$ (green) and $X^+\,^2E_{3/2}\leftarrow X\,^3A_2$ (orange) transitions in $Sb–CH_3$. IE of 8.01 eV ($X^+\,^2E_{1/2}\leftarrow X\,^3A_2$) and 8.43 eV ($X^+\,^2E_{3/2}\leftarrow X\,^3A_2$) are derived.

In the upper trace without pyrolysis, only the precursor signal at *m/z* 166 and 168, $Sb(CH_3)_3$ is seen. Note that Sb shows two isotopes, ^{121}Sb (57 %) and ^{123}Sb (43 %), causing a characteristic splitting of the mass peaks. In the lower trace, recorded at a pyrolysis temperature of 650 °C, several mass peaks are observed, with a pattern similar to the one reported above for $As(CH_3)_3$ pyrolysis. Again, peaks at *m/z* 151/153, 136/138 and 121/123 indicate sequential loss of methyl groups. Most likely, a minor concerted pathway associated with ethane or ethene loss is present as well. Here, CH_3 is not observed, due to its ionisation energy of 9.84 eV.[23] Notably, peaks at *m/z* 135 and 137 are missing, indicating the absence of $SbCH_2$. Bimolecular reactions in the pyrolysis reactor again lead to species that contain two, three or four Sb atoms. Due to the isotopic ratio, peaks overlap, but Sb_2^+, Sb_3^+, and Sb_4^+ are readily identified by their photoelectron spectra. Several smaller peaks result from multimers of methylated antimony clusters. For example, a peak centred slightly above *m/z* 300 most likely arises through dimerisation of dimethylantimony to $Sb_2C_4H_{12}^+$.[24]

Ms-TPE spectra for all species visible in the mass spectrum were obtained from the PEPICO data set. Apart from the Sb clusters, only the ms-TPE spectrum of $SbCH_3^+$ shows a vibrational structure. As photoelectron spectra of Sb clusters have been discussed previously,[17,18] they are only given in Figure S4, together with the unresolved spectra of other compounds ($Sb(CH_3)_2$, $[Sb(CH_3)_2]_2$). Figure 5 presents the ms-TPES of *m/z* 136, $SbCH_3^+$. Three bands can be observed, the first two at 7.9–8.4 eV and 8.4–8.8 eV have a very similar appearance and a well-resolved vibrational structure with a spacing of around 600 cm^{-1}. The third one is broad and unstructured and is assigned to an electronically excited state of $SbCH_3^+$, but might contain contributions from dissociative photoionisation of the precursor at higher photon energies.

Bands were simulated based on quantum chemical calculations on different levels of theory. The best simulation was obtained by DFT, using the ωB97-XD functional, a jorge-QZP basis set and the DKH method to include scalar relativistic effects. The calculated geometric parameters are summarised in Table 3. Computations also indicated a symmetry reduction from C_{3v} symmetry to C_s, comparable to $As–CH_3$ (see above). But again, the pseudorotational barrier of the methyl group of 150 meV (CCSD(T)) and the 950 meV zero point vibrational energy suggest that the methyl group can rotate freely, hence assignment as a $X^+\,^2E\leftarrow X\,^3A_2$ transition within the C_{3v} point group remains appropriate.

To obtain the spin-orbit splitting, we then performed NEVPT2 [11,11] calculations at the optimised geometry. Relativistic effects were again included using the DKH method.[20] An energy difference of 0.497 eV between the $^2E_{1/2}$ and $^2E_{3/2}$ states was calculated. The red line represents a simulation that is the sum of the individual contributions (green and orange line, respectively), assuming an intensity ratio of 1.4:1. Although the intensity ratio of the bands of almost 2:1 suggests the $^2E_{3/2}$ state to be the ground state, the calculations show that the $^2E_{1/2}$ is lower in energy, in accordance with Hund's third rule. Ionisation energies of 8.01 eV and 8.43 eV were derived for the $X^+\,^2E_{1/2}\leftarrow X\,^3A_2$ and $X^+\,^2E_{3/2}\leftarrow X\,^3A_2$ transitions, respectively. Thus, experimental and computed spin-orbit splitting agree within 70 meV.

The vibrational progression is characterised by a single mode that is assigned to the Sb–C stretch, $\tilde{\nu}_7^+$. In addition, the CH_3-wagging mode $\tilde{\nu}_9^+ = 470\ cm^{-1}$ appears with significant intensity in the simulation. While a 610 cm^{-1} spacing is apparent in the $^2E_{1/2}$ state, it is reduced to 580 cm^{-1} in the $^2E_{3/2}$

Table 3. Computed minimum energy geometries of $Sb–CH_3$ in its $X\,^3A_2$ and $Sb–CH_3^+$ in its $X^+\,^2E_{1/2}/^2E_{3/2}$ states.

	$X\,^3A_2$	$X^+\,^2E_{1/2}/^2E_{3/2}$
$R_{(SbC)}$/Å	2.13	2.05
$R_{(CH)}$/Å	3×1.09	2×1.09 1.10
$\theta_{(Sb–CH)}$/°	3×110	2×113 103
$\theta_{(HCH)}$/°	3×109	2×108 112

state. This indicates small differences in the potential energy surface of the two spin orbit states. A full characterisation requires accurate relativistic computations that are beyond the scope of the present work. Note that for its isomer $HSb{=}CH_2$ a photoionisation transition with an IE around 8.8 eV and a short vibrational progression with Franck-Condon factors comparable to $SbCH_3^+$ is predicted. Assuming a similar ionisation cross section, no evidence is visible for the presence of this isomer and its formation in the pyrolysis reactor.

Methyl transfer reactions and pnictinidene transfer reactions

The pyrolysis experiments performed with compounds $E(CH_3)_3$ (E–N–Bi) indicate the possibility of up to three homolytic E–CH_3 bond dissociations in these species. This is not only relevant for the application of such compounds in metalorganic chemical vapour deposition and related methodologies, but also in the context of methyl transfer reactions and pnictinidene transfer reactions in synthetic chemistry. For the bismuth compound $Bi(CH_3)_3$, we have previously shown that the release of methyl radicals is not only relevant under pyrolysis conditions, but can readily be detected by EPR spectroscopy at 60 °C in benzene solution using a nitrone as a spin trap.[2f] Furthermore, reaction of $Bi(CH_3)_3$, with the "bismuthinidene trapping reagent" diphenylsulfide, $(PhS)_2$, gave $Bi(CH_3)(SPh)_2$ in high isolated yield, suggesting that $BiCH_3$ might be generated and trapped under these conditions. In the context of this work, we aimed to evaluate the suitability of $As(CH_3)_3$ and $Sb(CH_3)_3$ as synthetically relevant sources of methyl radicals and methylpnictinidenes ($AsCH_3$ and $SbCH_3$, respectively) in the condensed phase (Scheme 1). In order to test the capability of $E(CH_3)_3$ (E–As, Sb) to release methyl radicals, $E(CH_3)_3$ was heated to 60 °C in toluene in the presence of phenyl-*N*-*tert*-butylnitrone as a radical trap, that is, under conditions analogous to those previously used for $Bi(CH_3)_3$ (Scheme 1, top). However, in the case of $As(CH_3)_3$ and $Sb(CH_3)_3$, only weak signals could be detected (about ten times weaker than in the bismuth case) and a clean methyl radical transfer could not be confirmed (see the Supporting Information). Similarly, no significant conversion could be detected, when $As(CH_3)_3$ and $Sb(CH_3)_3$ were reacted with $(PhS)_2$ under conditions that gave considerable isolated yields of $Bi(CH_3)(SPh)_2$, when the bismuth precursor was used (Scheme 1, bottom). These reactions demonstrate that the chemical robustness of compounds $E(CH_3)_3$ increases with decreasing atomic number of the central atom, making the lighter species less suitable for methyl radical transfer and pnictinidene transfer under mild conditions.

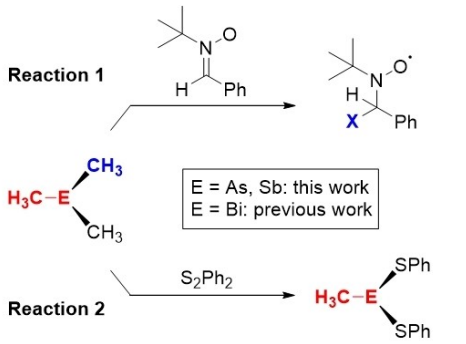

E	Reaction 1 (methyl radical transfer)	Reaction 2 (formal E-CH_3 transfer)
As	slow, unselective (X: ≥2 species)[a]	none
Sb		<5% conversion
Bi	good (X = CH_3)	42% isolated yield

Scheme 1. Reactions of $E(CH_3)_3$ with a nitrone (top) and $(PhS)_2$ (bottom) for E=As, Sb (this work) and E=Bi (previous work).[2f] For E=As, Sb, EPR spectroscopy indicated the presence of two or more closely related radical species (X=CH_3 plus at least one unidentified species) with a total intensity that was lower by a factor of approximately 10 compared to the case of E=Bi.

Discussion

With this work, we have now completed our investigation of the methyl and methylene compounds of all group 15 elements E by photoelectron spectroscopy. We will now discuss the trends that are apparent from the experiments. The IEs derived in this and previous work are summarised in Table 4.

From the table, several trends become obvious. As a first-row atom, nitrogen exhibits the largest structural diversity. The species HN=CH (*cis* and *trans*) and $H_2N{=}C$ were only observed for nitrogen, not for any of the higher congeners due to their high energy compared to $E{=}CH_2$. On the other hand, no N–CH_3 was observed. The overlap between the p orbitals on N and C permits the formation of stable double bonds, thus the formation of $HN{=}CH_2$ is strongly favoured. With increasing atomic radius, this overlap deteriorates, and methyl compounds become favoured. For E–P and As, both structures have been observed. In the case of E–P, the $HP{=}CH_2$ isomer is lower in energy by $\Delta_f H(0\,K) = 0.65$ eV/63 kJ mol^{-1} and the P–CH_3 photoelectron signal has consequently been weak.[2e] For E–As, the $HAs{=}CH_2$ isomer is only 136 meV more stable than As–CH_3, so both isomers show a comparable stability and appear with comparable intensity in the photoelectron spectrum (Figure 2). Finally, for E–Sb and Bi, only the E–CH_3 isomer is visible. All E–CH_3 congeners have a triplet ground state and are thus biradicals. Going from As to Sb thus leads to a change in the

Table 4. Ionisation energies of methyl- and methylene-compounds of group 15 elements E observed by threshold photoelectron spectroscopy.

	Energy/eV				
E	HE=CH	$H_2E{=}C$	$E{=}CH_2$	$HE{=}CH_2$	E–CH_3
N[5]	11.72 (*cis*) 12.65 (*trans*)	11.21 ($^3A''$)[a]	12.32 ($^3A_2$)	9.99	–
P[2e]	–	–	8.80 ($^1B_2$)	10.07	8.91
As	–	–	8.61 ($^1B_2$)	9.61	8.70
Sb	–	–	–	–	8.14
Bi[2f]	–	–	–	–	7.88

[a] A stable singlet cation has been computed, but not experimentally observed.

preferred bonding situation. This is surprising, because the major changes in the electronic structure occur between P and As (**3d** shell filled) and Sb and Bi (**4f** shell filled).

For all E–CH_3 species we find a symmetry reduction upon ionisation in the computations, regardless of the computational level. The CH_3 group is slightly tilted, and the C–H bonds become inequivalent. In the related Bi–CH_3, the distortion was rationalised by antibonding interactions between the unpaired electron at the Bi centre and the bonding electrons of the two C–H bonds, which are approximately aligned with the singly occupied p-type orbital. The geometric distortion should lead to a splitting of the ^{2}E ionic ground state into ^{2}A″ and ^{2}A′ components. In the TPES of Bi–CH_3 such a splitting is evident in the spectrum of the lower spin-orbit component, however, there is no evidence in the spectra of the lower congeners. For Sb–CH_3 and As–CH_3, the zero point vibrational energy suffices to overcome the barrier to internal rotation (see above), so a ^{2}E ionic ground state results and a similar situation can be assumed for E–P.

Increasing the nuclear charge from N to Bi also increases spin-orbit (SO) coupling, which should lead to a SO splitting of the electronic ground state of the ion. While SO splitting is negligible in P–CH_3, it is so large in Bi–CH_3 that the spin-orbit excited states were outside the investigated energy range. Preliminary computations yielded a value of $\Delta E_{SO} = 0.99$ eV. This leaves As–CH_3 and Sb–CH_3 as the most challenging cases. Here, the magnitude of SO splitting permits to observe both SO components in the cation. The experimentally observed splitting is $\Delta E_{SO} = 0.20$ eV for E=As and $\Delta E_{SO} = 0.42$ eV for E=Sb. The value for Sb–CH_3^+ compares well with $\Delta E_{SO} = 0.625$ eV for I–CH_3^+,[25] whereas the value for As–CH_3^+ is surprisingly high. According to Hund's third rule, the $^2E_{1/2}$ state should be lower in energy than the $^2E_{3/2}$ state, because the degenerate *e*-orbitals are less than half-filled (one electron in Sb–CH_3). On the other hand, due to its twofold degeneracy, the $^2E_{3/2}$ state should be more intense by a factor of approximately two. In Figures 4 and 5 it is evident that the low energy band is more intense and the intensity ratio would approximately match a $^2E_{3/2}$ ground state. However, computations show that the ionic ground state is $^2E_{1/2}$, in accordance with Hund's rules. Although these rules were originally formulated for atoms, the prediction is also valid in our cases. Note that the most important mechanism for intensity perturbations, spin-orbit autoionisation, would increase the intensity of the upper spin-orbit component.

In contrast to E–CH_3, the electronic ground state of the HE=CH_2 isomer is always a singlet. In HN=CH_2, the electron is ejected from a non-bonding orbital located at the nitrogen atom, while in HP=CH_2 and HAs=CH_2 the ionic ground state corresponds to ionisation from a π-orbital located at the E=C double bond. Consequently, the TPES spectra are dominated by a long bending mode progression in HN=CH_2, while E=CH_2 stretch and out-of-plane bends dominate in HP=CH_2 and HAs=CH_2.

The trend in the methylene compounds E=CH_2 parallels the one for HE=CH_2. Neither Sb=CH_2 nor Bi=CH_2 have been observed, while P=CH_2 and As=CH_2 are identified in the spectra. However, isolable compounds, described as stiba-alkenes and bisma-alkenes, have recently been reported using carbodicarbone ligands.[26] Interestingly, for E=CH_2 the spin multiplicity changes. For N=CH_2, a triplet ground state was identified in the cation, while the singlet cation was found to be a transition state to linear $HNCH^+$ on the potential energy surface. For E=P and As, E=CH_2^+ was identified to be a singlet ground state $X^+\,^1A_1$. The simulation of the $X^+\,^1A_1 \leftarrow X\,^2B_2$ transition of As=CH_2 underestimated the intensity of several vibrationally excited states in both molecules, while the $A^+\,^3A_2 \leftarrow X\,^2B_2$ transition was simulated well. A similar effect was observed previously for P=CH_2.[2e] Possible reasons for the deviations between experimental and computed intensities are either an intensity enhancement by autoionisation or the rather flat potential in the ionic ground state.

Conclusion

Threshold photoelectron spectra of reactive low-valent organoarsenic and organoantimony compounds have been investigated by using synchrotron radiation. Vibrationally resolved spectra were recorded for As–CH_3, HAs=CH_2, As=CH_2 and Sb–CH_3. The methyl compounds E–CH_3 (E–As, Sb) showed spin-orbit splitting in the cationic ground state, values of $\Delta E_{SO} = 0.20$ and 0.42 eV were derived for E–As and E–Sb, respectively. While ΔE_{SO} is in line with that of related compounds for Sb–CH_3^+, it is surprisingly large for As–CH_3^+. In both compounds, the $^2E_{1/2}$ state is lower in energy, in accordance with Hund's rules. Ionisation energies of IE(As–CH_3/$^2E_{1/2}$) = 8.70 eV and IE(Sb–CH_3/$^2E_{1/2}$) = 8.01 eV were obtained with error bars of ± 20 meV, and energies for the Franck-Condon active modes were determined. While for antimony Sb–CH_3 was the only stable isomer, for arsenic we also identified HAs=CH_2 with an IE(HAs=CH_2) = 9.61 eV and the methylene compound As=CH_2 with an IE(As=CH_2) = 8.61 eV. For the latter molecule, simulating the spectrum turned out to be difficult, either due to intensity perturbations by autoionisation or due to a rather flat cationic potential energy surface. This work completes a series of investigations on the reactive methyl compounds of the group 15 elements. While for E–N only species with N=C multiple bond character were observed, for Sb and Bi only E–CH_3 in a triplet ground state was identified. For E–P, As, on the other hand, both isomers were observed in the spectra. The increasing bond length $R_{(EC)}$ results in a smaller overlap between the p orbitals of E and carbon, disfavouring the formation of a (formal) double bond. In the condensed phase, neither As$(CH_3)_3$ nor Sb$(CH_3)_3$ is an efficient methyl transfer or pnictinidene transfer reagent, while for Bi$(CH_3)_3$ methyl release was detected in benzene solution by EPR spectroscopy.

These findings contribute to a detailed mapping of the accessibility, geometry, and electronic structure of the isomers of the low-valent, high-energy species ECH_3 and ECH_2 (E–N–Bi) and will thus be valuable for the design of precursors in materials science as well as methyl and pnictinidene transfer reagents.

Experimental Section

All species were characterised by using the double imaging photoelectron photoion coincidence setup (CRF-PEPICO) at the vacuum ultraviolet (VUV) beamline of the Swiss Light Source (SLS) at the Paul Scherrer Institute, Villigen (Switzerland). A detailed description has been published elsewhere,[27] therefore only a brief overview of the setup is given here. Synchrotron radiation provided by a bending magnet is collimated by a mirror and dispersed vertically by a plane grating. The light is guided through a Ne/Ar/Kr gas mixture to suppress higher order radiation. The photon energy was calibrated on the 11 s'–13 s' autoionisation lines of argon in both first and second order of the grating.

The reactive species were generated by introducing $As(CH_3)_3$ or $Sb(CH_3)_3$ vapor, seeded in argon through a nozzle with 0.1 mm diameter into a pyrolysis reactor. The gas flow and the precursor concentration in the gas mixture were controlled by two mass flow controllers. The gas mixture was pyrolysed in a SiC tube, resistively heated to 600–700 °C. The pyrolysis products form an effusive molecular beam and enter the experimental chamber through a 2 mm skimmer.[28] Here the molecular beam is crossed by the synchrotron radiation for ionisation. The resulting photoelectrons and photoions were extracted in opposite directions in a constant 218 V cm^{-1} electric field. Photoelectrons were velocity-map-imaged onto a Roentdek DLD40 delay line detector while the cations were detected in a Wiley-McLaren-type time-of-flight (TOF) spectrometer. Threshold photoelectrons were selected in the centre of the detector with an energy resolution better than 4 meV and the contributions of hot electrons were subtracted.[29] Photoions and photoelectrons were collected in a multiple-start/multiple-stop coincidence scheme.[30] Due to the insufficient expansion cooling, ms-TPES recorded from pyrolysis reactors, mostly suffer from broadening by hot and sequence band transitions. A reduction of these can be achieved by integrating only the room temperature background velocity component in the ions' VMI as was recently shown.[31–32] The resulting mass-selected threshold photoelectron (ms-TPE) spectra were corrected for photon flux and the ionisation energy in addition corrected for the Stark shift.

$As(CH_3)_3$ was synthesised as follows:[33] To a three-necked flask equipped with a dropping funnel with pressure compensation and an adapter for inert gas/vacuum, methylmagnesium bromide (1.0 M in nBu_2O, 95.3 mL, 95.3 mmol) was added. A solution of $AsBr_3$ (10.0 g, 31.8 mmol) in nBu_2O (20 mL) was added dropwise over 2 h at 0 °C. After complete addition, the reaction mixture was stirred for a further 2 h at 0 °C then for 16 h at ambient temperature. The dropping funnel was removed and a Vigreux column ($h = 19$ cm, $Ø = 3$ cm) equipped with a distillation apparatus and a Schlenk tube was added to the three-necked flask. The reaction mixture was distilled at atmospheric pressure and an oil bath temperature of 90 °C. The receiver Schlenk tube was cooled with liquid nitrogen to collect the $AsMe_3$ distillate. Yield: 3.26 g, 27.2 mmol, 85% (containing < 3 mol% nBu_2O). Boiling point: 53–55 °C. Analytical data (such as NMR spectra) were in agreement with the literature.[33] ^{1}H NMR (400 MHz, C_6D_6): $\delta = 0.76$ ppm (s, 9H, CH_3).

$Sb(CH_3)_3$ was synthesised as follows:[33] Methylmagnesium bromide (3.0 M in Et_2O, 86.6 mmol, 29.8 mL) was added to a suspension of $SbCl_3$ (6.82 g, 29.9 mmol) in diethyl ether (100 mL) at 0 °C. The reaction mixture was stirred at 0 °C for 15 min, then 1.5 h at ambient temperature. The suspension was filtered, and diethyl ether was removed partially by distillation at 50 °C (oil bath temperature). The residue was distilled at 90 °C and 5×10^{-3} mbar to give $SbMe_3$ as a colourless oil. Yield: 1.40 g, 8.07 mmol, 27% (containing 10 mol% Et_2O). Analytical data (such as NMR spectra) were in agreement with the literature.[33] ^{1}H NMR (400 MHz, C_6D_6): $\delta = 0.60$ ppm (s, 9H, CH_3).

Ionisation energies (IE), geometries and vibrational frequencies were computed on different levels of theory using ORCA[34] and the Gaussian 16 suite of programs.[35] IEs were obtained by subtracting the neutral molecule's energy from the cation's energy, including zero point energy contributions. Based on the computed geometries and frequencies, the photoelectron spectra were simulated by ezSpectrum,[36] which computes Franck-Condon factors (FCF) for the transitions. The resulting stick spectra were convolved with a Gaussian function of 25 meV full width at half maximum height.

Supporting Information

Additional references are cited within the Supporting Information.[37–40]

Acknowledgements

The experiments were performed at the VUV beamline of the Swiss Light Source, located at the Paul Scherrer Institute (PSI). The work was financially supported by the Deutsche Forschungsgemeinschaft, contract FI575/13-2 and LI2860/5-1, and by the LOEWE program. This project has received funding from the European Research Council (ERC) under the European Union's Horizon 2020 research and innovation program (grant agreement no. 946184). Open Access funding enabled and organized by Projekt DEAL.

Conflict of Interests

The authors declare no conflict of interest.

Data Availability Statement

The data that support the findings of this study are available in the supplementary material of this article.

Keywords: biradicals · methylpnictinidenes · methylantimony · methylarsene · threshold photoelectron spectroscopy

[1] a) N. M. Leonard, L. C. Wieland, R. S. Mohan, *Tetrahedron* **2002**, *58*, 8373–8397; b) W. Jerzembeck, H. Bürger, L. Constantin, L. Margulès, J. Demaison, J. Breidung, W. Thiel, *Angew. Chem. Int. Ed.* **2002**, *41*, 2550–2552; *Angew. Chem.* **2002**, *114*, 2659–2661; c) D. H. R. Barton, J.-P. Finet, *Pure Appl. Chem.* **1987**, *59*, 937–946.
[2] a) P. P. Power, *Chem. Rev.* **1999**, *99*, 3463–3504; b) N. Tokitoh, *J. Organomet. Chem.* **2000**, *611*, 217–227; c) C. Jones, *Coord. Chem. Rev.* **2001**, *215*, 151–169; d) H. J. Breunig, L. Balázs, *Organometallics* **2004**, *23*, 304–310; e) D. P. Mukhopadhyay, M. Gerlach, S. Hartweg, I. Fischer, J.-C. Loison, *Phys. Chem. Chem. Phys.* **2022**, *24*, 10993–10999; f) D. P. Mukhopadhyay, D. Schleier, S. Wirsing, J. Ramler, D. Kaiser, E. Reusch, P. Hemberger, T. Preitschopf, I. Krummenacher, B. Engels, I. Fischer, C. Lichtenberg, *Chem. Sci.* **2020**, *11*, 7562–7568; g) O. J. Scherer, *Angew. Chem. Int. Ed.* **1985**, *24*, 924–943; *Angew. Chem.* **1985**, *97*, 905–924.
[3] L. Dostál, *Coord. Chem. Rev.* **2017**, *353*, 142–158.
[4] T. Baer, P.-M. Guyon, in *High Resolution Laser Photoionisation and Photoelectron Studies*, (Eds.: C. Y. Ng, T. Baer, I. Powis), Wiley, New York, **1995**.

[5] F. Holzmeier, M. Lang, K. Hader, P. Hemberger, I. Fischer, *J. Chem. Phys.* **2013**, *138*, 214310.
[6] R. Waterman, T. D. Tilley, *Angew. Chem.* **2006**, *118*, 2992–2995; *Angew. Chem. Int. Ed.* **2006**, *45*, 2926–2929.
[7] a) H. W. Moon, J. Cornella, *ACS Catal.* **2022**, *12*, 1382–1393; b) Y. Pang, M. Leutzsch, N. Nöthling, F. Katzenburg, J. Cornella, *J. Am. Chem. Soc.* **2021**, *143*, 12487–12493.
[8] a) H. Lei, J. Chen, Z. Tan, G. Fang, *Solar RRL* **2019**, *3*, 1900026; b) R. M. Biefeld, *Mater. Sci. Eng. R* **2002**, *36*, 105–142; c) Mamta, Y. Singh, K. K. Maurya, V. N. Singh, *Sol. Energy Mater. Sol. Cells* **2021**, *230*, 111223.
[9] N. Bahlawane, F. Reilmann, S. Schulz, D. Schuchmann, K. Kohse-Höinghaus, *J. Am. Soc. Mass Spectrom.* **2008**, *19*, 1336–1342.
[10] A. Chrostowska, A. Dargelos, V. Lemierre, J.-M. Sotiropoulos, P. Guenot, J.-C. Guillemin, *Angew. Chem. Int. Ed.* **2004**, *43*, 873–875; *Angew. Chem.* **2004**, *116*, 891–893.
[11] a) V. Lemierre, A. Chrostowska, A. Dargelos, H. Chermette, *J. Phys. Chem. A* **2005**, *109*, 8348–8355; b) V. Tognetti, C. Adamo, P. Cortona, *Chem. Phys.* **2007**, *337*, 161–167.
[12] Z. Havlas, M. Kyvala, J. Michl, *Collect. Czech. Chem. Commun.* **2003**, *68*, 2335–2343.
[13] K. D. Dobbs, J. E. Boggs, A. H. Cowley, *Chem. Phys. Lett.* **1987**, *141*, 372–375.
[14] T. Baer, R. P. Tuckett, *Phys. Chem. Chem. Phys.* **2017**, *19*, 9698–9723.
[15] a) I. Fischer, S. T. Pratt, *Phys. Chem. Chem. Phys.* **2022**, *24*, 1944–1949; b) P. Hemberger, A. Bodi, T. Bierkandt, M. Köhler, D. Kaczmarek, T. Kasper, *Energy Fuels* **2021**, *35*, 16265–16302.
[16] B. Hornung, A. Bodi, C. I. Pongor, Z. Gengeliczki, T. Baer, B. Sztáray, *J. Phys. Chem. A* **2009**, *113*, 8091–8098.
[17] L. S. Wang, Y. T. Lee, D. A. Shirley, K. Balasubramanian, P. Feng, *J. Chem. Phys.* **1990**, *93*, 6310–6317.
[18] a) L. S. Wang, B. Niu, Y. T. Lee, D. A. Shirley, E. Ghelichkhani, E. R. Grant, *J. Chem. Phys.* **1990**, *93*, 6318–6326; b) L. S. Wang, B. Niu, Y. T. Lee, D. A. Shirley, E. Ghelichkhani, E. R. Grant, *J. Chem. Phys.* **1990**, *93*, 6327–6333.
[19] R. Sarkar, P.-F. Loos, M. Boggio-Pasqua, D. Jacquemin, *J. Chem. Theory Comput.* **2022**, *18*, 2418–2436.
[20] M. Reiher, *Theor. Chem. Acc.* **2006**, *116*, 241–252.
[21] P. T. Murray, T. Baer, *Int. J. Mass Spectrom. Ion Phys.* **1979**, *30*, 165–174.
[22] S. T. Pratt, P. M. Dehmer, J. L. Dehmer, *J. Chem. Phys.* **1992**, *97*, 3038–3049.
[23] a) B. K. Cunha de Miranda, C. Alcaraz, M. Elhanine, B. Noller, P. Hemberger, I. Fischer, G. Garcia, H. Soldi-Lose, B. Gans, L. A. Viera Mendez, S. Boye-Peronne, S. Douin, J. Zabka, P. Botschwina, *J. Phys. Chem. A* **2010**, *114*, 4818–4830; b) J. A. Blush, P. Chen, R. T. Wiedmann, M. G. White, *J. Chem. Phys.* **1993**, *98*, 3557–3559.
[24] S. Yamago, T. Yamada, M. Togai, Y. Ukai, E. Kayahara, N. Pan, *Chem. Eur. J.* **2009**, *15*, 1018–1029.
[25] A. Strobel, I. Fischer, A. Lochschmidt, K. Müller-Dethlefs, V. E. Bondybey, *J. Phys. Chem.* **1994**, 2024–2032.
[26] a) L. S. Warring, J. E. Walley, D. A. Dickie, W. Tiznado, S. Pan, R. J. Gilliard, Jr., *Inorg.* **2022**, *61*, 18640–18652; b) J. E. Walley, L. S. Warring, G. Wang, D. A. Dickie, S. Pan, G. Frenking, R. J. Gilliard Jr, *Angew. Chem.* **2021**, *133*, 6756–6764; *Angew. Chem. Int. Ed.* **2021**, *60*, 6682–6690.
[27] a) M. Johnson, A. Bodi, L. Schulz, T. Gerber, *Nucl. Instrum. Methods Phys. Res. A: Accel. Spectrom. Detect. Assoc. Equip.* **2009**, *610*, 597–603; b) A. Bodi, M. Johnson, T. Gerber, Z. Gengeliczki, B. Sztáray, T. Baer, *Rev. Sci. Instrum.* **2009**, *80*, 034101; c) A. Bodi, P. Hemberger, T. Gerber, B. Sztáray, *Rev. Sci. Instrum.* **2012**, *83*, 083105; d) B. Sztáray, K. Voronova, K. G. Torma, K. J. Covert, A. Bodi, P. Hemberger, T. Gerber, D. L. Osborn, *J. Chem. Phys.* **2017**, *147*, 013944.
[28] D. W. Kohn, H. Clauberg, P. Chen, *Rev. Sci. Instrum.* **1992**, *63*, 4003–4005.
[29] B. Sztáray, T. Baer, *Rev. Sci. Instrum.* **2003**, *74*, 3763–3768.
[30] A. Bodi, B. Sztáray, T. Baer, M. Johnson, T. Gerber, *Rev. Sci. Instrum.* **2007**, *78*, 084102.
[31] C. Fernholz, A. Bodi, P. Hemberger, *J. Phys. Chem. A* **2022**, *126*, 9022–9030.
[32] P. Hemberger, X. Wu, Z. Pan, A. Bodi, *J. Phys. Chem. A* **2022**, *126*, 2196–2210.
[33] I. Fleming, S. V. Ley, *Science of Synthesis: Houben-Weyl Methods of Molecular Transformations: Category 1 Organometallics (Compounds of Group 15 (As, Sb, Bi) and Silicon Compounds)*, 1st ed., Thieme, Stuttgart, **2001**.
[34] F. Neese, *Wiley Interdiscip. Rev.: Comput. Mol. Sci.* **2022**, *12*, e1606.
[35] M. J. Frisch, G. W. Trucks, H. B. Schlegel, G. E. Scuseria, M. A. Robb, J. R. Cheeseman, G. Scalmani, V. Barone, G. A. Petersson, H. Nakatsuji, X. Li, M. Caricato, A. V. Marenich, J. Bloino, B. G. Janesko, R. Gomperts, B. Mennucci, H. P. Hratchian, J. V. Ortiz, A. F. Izmaylov, J. L. Sonnenberg, Williams, F. Ding, F. Lipparini, F. Egidi, J. Goings, B. Peng, A. Petrone, T. Henderson, D. Ranasinghe, V. G. Zakrzewski, J. Gao, N. Rega, G. Zheng, W. Liang, M. Hada, M. Ehara, K. Toyota, R. Fukuda, J. Hasegawa, M. Ishida, T. Nakajima, Y. Honda, O. Kitao, H. Nakai, T. Vreven, K. Throssell, J. A. Montgomery Jr., J. E. Peralta, F. Ogliaro, M. J. Bearpark, J. J. Heyd, E. N. Brothers, K. N. Kudin, V. N. Staroverov, T. A. Keith, R. Kobayashi, J. Normand, K. Raghavachari, A. P. Rendell, J. C. Burant, S. S. Iyengar, J. Tomasi, M. Cossi, J. M. Millam, M. Klene, C. Adamo, R. Cammi, J. W. Ochterski, R. L. Martin, K. Morokuma, O. Farkas, J. B. Foresman, D. J. Fox, *Gaussian 09, Revision A.02*, Gaussian Inc. Wallingford, CT, **2016**.
[36] S. Gozem, A. I. Krylov, *Wiley Interdiscip. Rev.: Comput. Mol. Sci.* **2022**, *12*, e1546.
[37] a) J. M. Dyke, S. Elbel, A. Morris, J. C. H. Stevens, *J. Chem. Soc. Faraday Trans. 2* **1986**, *82*, 637–645
[38] P. Hemberger, J. A. van Bokhoven, J. Pérez-Ramírez, A. Bodi, *Catal. Sci. Technol.* **2020**, *10*, 1975–1990.
[39] S. Elbel, J. Kudnig, M. Grodzicki, H. J. Lempka, *Chem. Phys. Lett.* **1984**, *109*, 312–316.
[40] S. Stoll, A. Schweiger, *J. Magn. Reson.* **2006**, *178*, 42–55.

Manuscript received: February 27, 2023
Accepted manuscript online: March 30, 2023
Version of record online: May 2, 2023